Carbohydrate Polymers 191 (2018) 103–111

Contents lists available at ScienceDirect

Carbohydrate Polymers

journal homepage: www.elsevier.com/locate/carbpol

Preparation and characterization of nanocomposite films from oil palm pulp nanocellulose/poly (Vinyl alcohol) by casting method

Mohammad Asad[a,b,c], Naheed Saba[d], Abdullah M. Asiri[a,b], M. Jawaid[d,*], Eti Indarti[c,e], W.D. Wanrosli[c,*]

[a] Chemistry Department, Faculty of Science, King Abdulaziz University, Jeddah 21589, Saudi Arabia
[b] Center of Excellence for Advanced Materials Research (CEAMR), King Abdulaziz University, Jeddah 21589, Saudi Arabia
[c] School of Industrial Technology, Universiti Sains Malaysia, 11800 USM, Penang, Malaysia
[d] Laboratory of Biocomposite Technology, Institute of Tropical Forestry and Forest Products (INTROP), Universiti Putra Malaysia, 43400 Serdang, Selangor, Malaysia
[e] Agricultural Product Technology Dept., Faculty of Agriculture, Syiah Kuala University, Banda Aceh 23111, Indonesia

ARTICLE INFO

Keywords:
Oil palm pulp nanocellulose
Nanocomposite films
Poly (vinyl) alcohol
TEMPO-oxidation
Thermal analysis

ABSTRACT

TEMPO-oxidize nanocellulose (TONC) suspension has been obtained from total chlorine free (TCF) oil palm empty-fruit-bunches (OPEFB) pulp using 4-acetamido-TEMPO (2,2,6,6-tetramethyl piperidin-1-oxyl) mediated oxidation with sodium hypochlorite and sodium bromide in water at 25 °C and pH 10. TONC suspension with varied content from 0.5 to 6% (w/w) reinforced polyvinyl alcohol (PVA) polymer based nanocomposite films were prepared by the casting method. The structural interaction between the TONC and PVA was characterized by the Fourier transform infrared (FT-IR) spectroscopy, nuclear magnetic resonance (NMR) spectroscopy, X-ray diffraction (XRD) and scanning electron microscopy (SEM). It was found that the 4% (w/w) TONC content reinforced nanocomposite exhibited the highest tensile strength and modulus with an increase of 122% and 291% respectively, compared to PVA while the elongation at break decreased about 42.7%. Thermal stability of PVA based nanocomposite films was improved after incorporation of TONC. Incorporation of TONC in PVA film increases its crystallinity due to strongly linking between the hydroxyl groups of materials however considerable decreases beyond 2 wt% loading are observed. TONC incorporation beyond 2 wt% also reduces the melting temperature peaks and enthalpy of nanocomposite films. FT-IR spectra, NMR and SEM indicate that there is interaction between the TONC and PVA.

1. Introduction

Nanocellulose has been considered a most abundant and inexpensive biopolymer with a wide variety of applications in different areas (Brinchia, Cotana, Fortunati, & Kenny, 2013). The promising applications of nanocellulose have been biodegradability, sustainability, high biocompatibility and most significant for the reinforcement polymeric matrix into nanocomposite materials (Ferraz et al., 2012; Korhonen, Kettunen, Ras, & Ikkala, 2011; Mulligan, 2005; Siqueira, Bras, & Dufresne, 2009). It has vast significance in medical, food, pharmaceutical industries, nanotechnology and also in several materials that are widely used commercially (Khan, Huq, Khan, Riedl, & Lacroix, 2014; Yan et al., 2014). Due to less cost and environmentally safe property, it can be also replace synthetic or petrochemical-based materials in many applications (Brinchi et al., 2013). Earlier, nanocellulose has been isolated from various kinds of cellulosic sources as cotton, wood, plant, animals, bacteria, algae and oil palm biomass (OPB) (Hassan, Bras, Hassan, Silard, & Mauret, 2014; Wanrosli, Rohaizu, & Ghazali, 2011). At a conservative estimate, for every tons of palm oil produced from a fresh fruit bunch, approximately 1 tons of empty fruit bunch (EFB), 0.7 tons of palm fibers, 0.3 tons of palm kernels and 0.3 tons of palm shells are generated, which amounts to a total palm biomass of 2.3 tons (Chang, 2014). These residues represent an abundant, inexpensive and readily available source of renewable lignocellulosic biomass which can be exploited for use in various applications such as reinforcement in nanocomposites.

Nowadays, nanomaterials are used in packaging industries like food stuff due to degradability and enhance to the quality of new bio-based packaging materials such as edible and biodegradable films from renewable resources (Sorrentino, Gorrasi, & Vittoria, 2007; Tharanathan, 2003). It has potentiality for the preparation of composite films because its biodegradability considered as a promising solution to the environmental pollution of synthetic polymer packaging (Su, Huang, Yuan, Wang, & Li, 2010). Until now biodegradable films has been used

* Corresponding authors.
E-mail addresses: jawaid_md@yahoo.co.in, jawaid@upm.edu.my (M. Jawaid), wanrosli@usm.my (W.D. Wanrosli).

https://doi.org/10.1016/j.carbpol.2018.03.015
Received 22 December 2017; Received in revised form 20 February 2018; Accepted 9 March 2018
Available online 11 March 2018
0144-8617/

for packaging extremely limited due to weak barrier and mechanical properties shown by natural polymers. Hence, the natural polymers as cellulose was chemically modified using the TEMPO oxidation and frequently reinforced with a matrix as poly(vinyl alcohol) for their improvement of various properties and applications in further circumstances (Lin, Bruzzese, & Dufresne, 2012; Ng et al., 2015).

Polyvinyl alcohol (PVA) is a semi-crystalline, fully biodegradable, non-toxic, biocompatible and water soluble synthetic polymer which is mainly composed of C—C and has excellent composite film casting property for packaging materials (Chiellini, Cinelli, Imam, & Mao, 2001; Zhang, Burgar, Lourbakos, & Beh, 2004). It has potential ability to interact with the hydrophilic surfaces of the biomaterials due to the strong hydrogen bonding and established in suitable combinations with cellulose or nanocellulose for produce green nanocomposites (Lee et al., 2012). It is incorporated into nanocellulose finds various significant applications in the field of pharmaceuticals, medicine and packaging (Rahman, Afrin, & Haque, 2014).

In the present work, the nanocellulose crystals (TONC) were isolated using the TEMPO-oxidized process from OPEFB cellulose, which was prepared via a chlorine-free bleaching sequence (Leh, Rosli, Zainuddin, & Tanaka, 2008; Rosli, Leh, Zainuddin, & Tanaka, 2003). Usually, the C6 hydroxyls groups oxidized into carboxylate groups by the TEMPO treatment is shown in Fig. 1 (Isogai, Saito, & Fukuzumi, 2011). The TONC/PVA composite films were prepared by mixing TONC and PVA in distill water with various content ratios and subsequently cast in petri dishes, followed by drying of the mixtures. The structural, physical-chemical and mechanical properties were characterized and evaluated by scanning electron microscopy (SEM), field emission scanning electron microscopy (FESEM), Fourier transform infrared (FTIR) spectroscopy, nuclear magnetic resonance (^{13}C NMR), x-ray diffraction analysis (XRD), differential scanning calorimetry (DSC) and tensile testing.

2. Experimental

2.1. Materials

Oil palm empty fruit bunches (OPEFB) were obtained for use in this study from a local palm oil mill in Perak, Malaysia. Before pulping, the OPEFB was cut to approximately 2 inches long, which was then soaked and washed with distilled water to remove dirt and unwanted materials and air dried to average moisture content of 12.5% and stored in polyethylene bags. The chemicals used for pulping, bleaching, oxidation and composites such as sodium hydroxide (NaOH), magnesium sulfate ($MgSO_4$), hydrogen peroxide (H_2O_2), hydrochloric acid (HCl), 4-acetamido-TEMPO (2,2,6,6-tetramethylpiperidin-1-oxyl) 99.8%, sodium hypochlorite (NaClO), sodium chlorite ($NaClO_2$) 99.8%, sodium bromide (NaBr, 99.0%), acetic acid (CH_3COOH) 99.8%, ethanol, and polyvinyl alcohol (98%) were obtained from E. Merck (Germany).

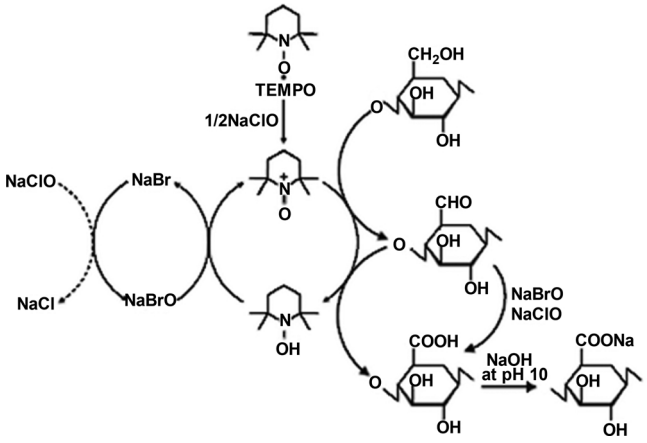

Fig. 1. Regioselective oxidation of cellulose by TEMPO-mediated oxidation (Isogai et al., 2011).

2.2. Methods

2.2.1. Preparation of OPEFB-TCF cellulose

OPEFB-TCF cellulose was prepared using the environmentally benign process as described by Wanrosli et al. (Wanrosli, Zainuddin, & Lee, 2004). Basically, it involves water pre-hydrolysis of the OPEFB fibers, followed by soda-anthraquinone pulping. The unbleached pulp was then bleached using a TCF sequence of oxygen (O), ozone (Z) and peroxide (P).

2.2.2. Preparation of TEMPO-oxidized nanocellulose (TONC)

OPEFB-TCF cellulose (10 g) was suspended in 1 L of distill water in a beaker, containing TEMPO (0.230 g), sodium bromide (0.5 g), and stirred for 5 min. The reaction was initiated by setting the ultrasonic water bath (model Branson 8510) at a frequency of 40 kHz and 320 W power output with circulating cooling water used to maintain the temperature at 25 °C. Additions of 60 mL sodium hypochlorite solution in the reaction mixture drop by drop, during the 1 h and continue stirring at 500 rmp for 4 h with controlled pH at 10 ± 0.2 by the addition of 0.5 M NaOH/HCl. The stirring was stopped and 100 mL ethanol was added to it. The oxidized slurry was neutralized by adding 0.5 M HCl, vacuum-filtered and thoroughly washed with distill water. The pulp was suspended in 500 mL of distill water in a glass bottle, 40 mL of sodium chlorite (34 g/L) and acetic acid (5 M) solutions added to it. The solution was kept in a water bath at 70 °C for 2 h, cooled at room temperature and washed with distill water. TEMPO-oxidized pulp was transferred in a beaker and sonicated (7 microtip limit) with 15 s interpose/min on ice bath and centrifuged at 3500 rmp for 1 h to separate the supernant containing TONC suspension from the unfibrillated and partially fibrillated fractions.

2.2.3. Preparation of TONC/PVA nanocomposite films

The solution of PVA (10 wt%) was prepared in distilled water and poured into a round bottom flask equipped with a condenser for 1 h stirring at 90 °C. TONC suspension was added to it in various concentrations 0.5, 1, 2, 4 and 6% (w/w) respectively. The mixtures were further stirred for 2 h and keep at room temperature for 0.5 h. The final suspensions were cast in polypropylene petri dishes and placed in a vacuum oven at the 50 °C for 48 h. The resulting films thus obtained were kept in the desiccators until the characterization.

2.3. Characterization techniques

2.3.1. Tensile properties

Tensile properties (tensile strength, Young's modulus and elongation at break) were performed on a TA-XT Plux Texture Analyzer. The tensile deformation was determined at a crosshead speed of 10 mm/min. The dimensions of the films according to the standard test method €N 150 527-2, 1996 was as follows: length 60 mm, width 30 mm, thickness 0.04 mm and load cell 30 kg. The measurements were performed at room temperature and calculated over five test samples, expressing the results as the mean value.

2.3.2. Differential scanning calorimetry (DSC)

DSC analysis was performed with a DSC-60 Instrument (Shimadzu D 60). Approximately 10 mg sample of the films was heated from 30 °C to 400 °C at a heating rate of

10 °C/min under nitrogen atmosphere. The DSC curves were used to determine the glass transition temperature, melting temperature and melting enthalpy. The degree of crystallinity (Xc) was calculated by using the following Eq. (1) (Frone, Berlioz, Chailan, & Panaitescu, 2013).

$$X\ c = \frac{\Delta H m}{w \times \Delta H mo} \times 100 \quad (1)$$

Where, (Xc) is the degree of crystallinity, (*w)* is the mass content of PVA in composite films, (ΔHm) is the enthalpy of melting (J g^{-1}), (ΔHmo) is the enthalpy of melting for 100% crystalline PVA considered to be 138.6 J g^{-1} (Peppas & Merrill, 1976).

2.3.3. Fourier transform infrared spectroscopy (FTIR)

FTIR spectra of the films were recorded on SMART OMNI-TRANSMISSION (Nicolet IS10 model) instrument. The resulting FTIR spectra were analyzed in functional groups occurred by the oxidation and compared the effects of nanocellulose filling into PVA, based on the intensity and shift of vibration bands. The films were cut around 3 cm and directly loaded for analyzed the observance of bands within the range of 4000–400 cm^{-1}.

2.3.4. ^{13}C nuclear magnetic resonance spectroscopy (NMR)

The solid ^{13}C NMR spectra of the films were recorded on a Bruker Avance III 400 MHz spectrometer. The chemical shifts are reported in parts per million (d-scale) used tetra methyl silane (TMS) as an external standard.

2.3.5. X-ray diffraction (XRD)

X-ray diffraction analyses were collected using a BRUKER AXS-D8 ADVANCE model Instrument. The generator operated at 40 kV and 30 mA. The films were scanned in steps of 0.0034° in a range of the diffraction angle 2θ = 10–40° with a Copper (CuKα) beam (wavelength 1.5406 Å). Crystallinity index was calculated by Eq. (2) (Segal, Creely, Martin, & Conrad, 1959).

$$\text{Crystallinity Index (\%)} = [(I_{cry} - I_{am})/I_{cry}] \times 100 \quad (2)$$

where, I_{cry} is the maximum intensity of the crystalline fraction at 2θ between 22° and 24°. I_{am} is the intensity in the valley between the peaks of the amorphous region at 2θ = 18.

2.3.6. Scanning electron microscopy (SEM)

SEM was used to investigate the morphology of the films by using a model Car1-Zeiss SMT Leo Supra 50 VP equipped with Oxford instrument energy dispersive. The samples were sputter-coated with a layer of gold using the sputtering technique.

3. Results and discussion

TEMPO-oxidized nanocellulose suspension (TONC) was isolated via a chemical and mechanical process using 4-acetamido-TEMPO (2,2,6,6-tetramethylpiperidin-1-oxyl)/NaBr/NaClO oxidation and ultrasonic treatment from OPEFB-TCF cellulose. In our previous study we reported the transmission electron microscopy images of TONC resembling rod-like crystalline morphology shown in Fig. 2 with an average length and width of 122 and 6 nm respectively (Rohaizu & Wanrosli, 2017). Suspension containing TONC was then incorporated into the PVA solution at various ratios of 0.5, 1, 2, 4 and 6% (w/w) for casting composite films. Effect of adding TONC on mechanical, structural, morphological, thermal stability and crystallinity was evaluated through tensile, *FT-IR*, *^{13}C NMR,* SEM, TGA, DSC and XRD respectively.

3.1. Tensile properties

Fig. 3(a–b) shows the tensile strength, Young's modulus, and elongation at break of TONC/PVA films at different TONC loadings. It was observed that tensile strength increase significantly from 63.2 to 140.3 MPa while Young's modulus increase from 1.01 to 3.95 GPa as the TONC content increases from 0.5 to 4% (w/w), representing 122% and 291% enhancement respectively compared to that of the PVA (control sample) which is a common phenomenon in lignocellulosic

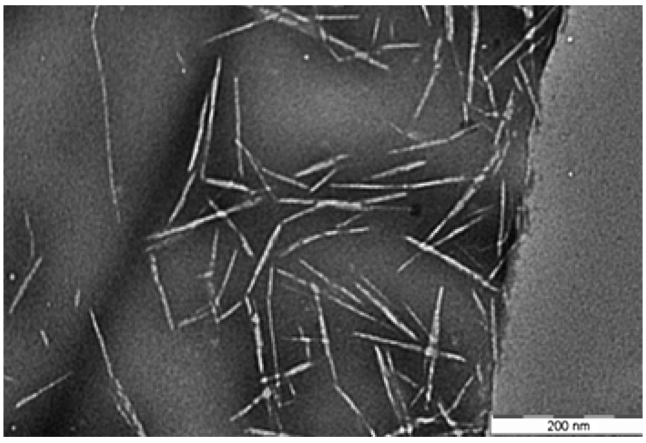

Fig. 2. TEM of TEMPO-oxidized nanocrystalline cellulose.

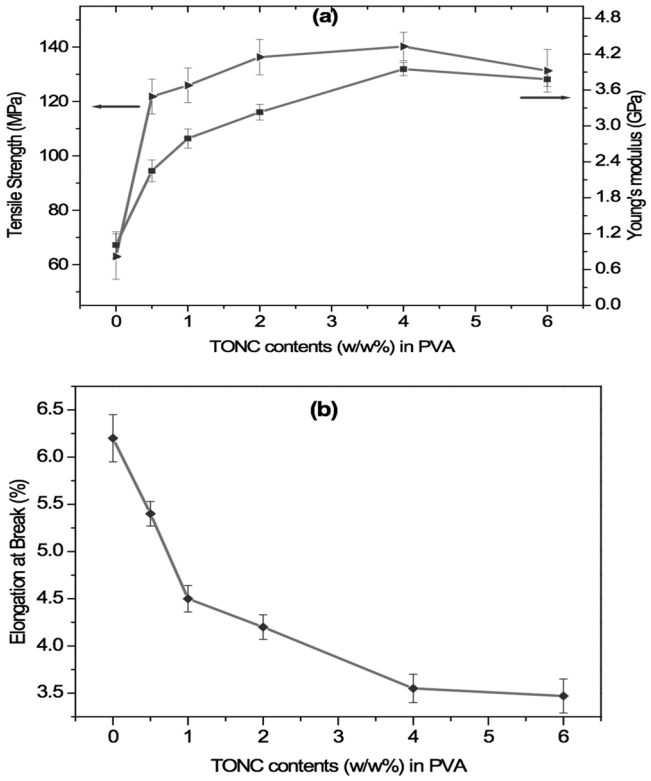

Fig. 3. Effect of TONC loadings on reinforced PVA-based composite films on (a) tensile strength and Young's modulus, (b) elongation at break.

fiber reinforced composites (Lee et al., 2009). This increase in the tensile properties has been ascribed as possibly due to the formation of a networked structure above percolation threshold resulting from increased hydrogen bonding between these materials due to the large surface area of the TONC (Azizi Samir, Alloin, & Dufresne, 2005; Siqueira et al., 2009). The phenomenal increase of Young's modulus has also been reported by Zimmermann et al. using cellulose fibrils isolated from sulphite pulp (Zimmermann, Pöhler, & Geiger, 2004).

At higher TONC loadings (6%), both of the mechanical properties start to experience a slight drop, which can be attributed to non-homogenous dispersion of the TONC in PVA matrix resulting from aggregation of the nanocellulose that decreases the tensile strength and Young's modulus (Lu, Wang, & Drzal, 2008). The elongation at break of the PVA based composites continuously decrease with the addition of TONC (Fig. 3b) reaching the lowest value at a 6% TONC addition with a reduction of 42.7%. Huq et al. also reported a decrease in elongation at

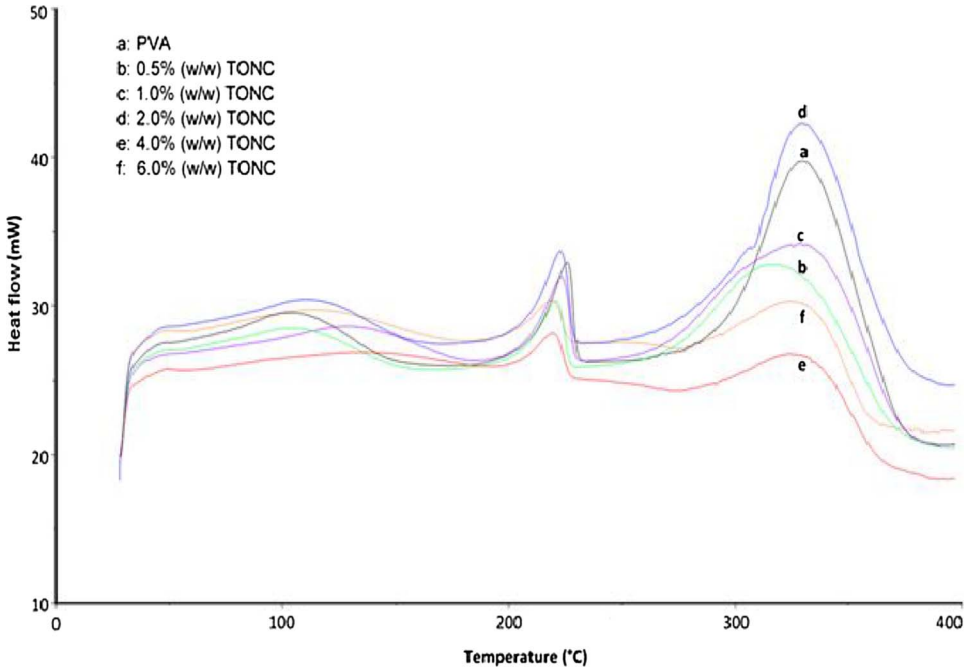

Fig. 4. DSC curves of TONC content reinforced PVA-based composite films.

break with the addition of nanocellulose in alginate based films (Huq et al., 2012). Overall addition of TONC below 6% to the PVA considerably results enhancements in tensile strength and modulus, as it is relatively rigid and stiffer material, thus they consequently alter or divert the applied stress resulting reduction in early or pre-fracture of the nanocomposite. Moreover, the presence of the rigid nanoparticles in the polymer matrix decreases the deformability of the interface between the two materials that will lead to a reduced segment mobility as a result of that the composite becomes more stiffer and harder hence shows lower elongation at break also.

3.2. Thermal properties

DSC curves of the TONC reinforced PVA-based composite films are presented in Fig. 4. Thermal stability data and calculated degree of crystallinity (Xc) of the composites are reported in Table 1. Fig. 4 clearly shows that the incorporation of TONC in PVA composite films increases the glass transition temperature (Tg) while reduces the melting temperatures (Tm). These composites exhibited the initial decomposition around 100 °C, which could be due to the result of water evaporation. The endotherms exhibited in the range of 200–350 °C which is indicating two melting peaks (Tm_1 and Tm_2) for treated and untreated TONC into PVA composites. The original melting temperature is considered at low melting temperature peak (Tm_1) in the range of 200–250 °C. It can be also expect that the other melting temperature peak (Tm_2) exceeding the 300 °C which is indicated degradation of cellulose by blending of components for casting composite films. The endothermic peak around 230 °C exhibited to the melting temperature of PVA composite (Park, Park, & Ruckenstein, 2001). It can be observed that PVA after the addition of 2% (w/w) TONC content exhibited the primary enhancement in melting enthalpy (ΔHm) of 61.89 J g^{-1} and crystallinity 45.56%, respectively.

Moreover, PVA exhibited the lower thermal stability after the addition of 0.5, 1, 4 and 6% (w/w) TONC contents. However, the melting temperature slightly decreased around 8 °C as compared to PVA (control sample) because of hydrogen bonding between these materials. Orts et al. also reported the melting temperature decreases with the increase of biopolymer content (Orts et al., 2007).

The DSC (Table 1) also clarify that the trend of overall melting temperature peaks (Tm_1 and Tm_2) and ΔH_m is quite similar to that of χ_c. Furthermore melting point of the nanocomposites films does not depend on the TONC contents loading up to 2 wt%, also χ_c is nearly constant with TONC contents up to 2 wt%. But the incorporation of TONC filler beyond 2 wt% greatly reduces the values of melting temperature peaks, ΔH_m and crystallinity.

Recently researchers in their study elaborated the thermal properties of the incorporated cellulose nanocrystals (CNCs) in PVA composites, where increasing the CNCs loading beyond 8% hinder the PVA polymer chains regular rearrangements which lowered the crystallization of PVA (Voronova, Surov, Guseinov, Barannikov, & Zakharov, 2015). From Table 1, it is also evident that Xc (%) of PVA shows increment from 0% to 2% TONC contents addition, as it does not interrupt the regular packing of molecule chain of PVA, while the further addition of TONC beyond 2% a considerable reduction in Xc (%) are observed owing to existence of couplet of factors like agglomeration of TONC at higher concentration, hydrophilic properties of both TONC and PVA, crystallinity of PVA and the consequent decrease in ΔH_m until 6% TONC contents. The statements are in agreement to other reported work (Sun, Lu, Liu, Zhang, & Zhang, 2014; Zhang et al., 2014).

Table 1
DSC results of PVA and composite films with various TONC contents.

Sample	Tg (°C)	Tm_1 (°C)	Tm_2 (°C)	ΔHm (J g^{-1})	Xc (%)
PVA	49.22	225.64	330.79	59.26	42.75
0.5% TONC/PVA	50.52	220.85	320.45	50.22	36.41
1% TONC/PVA	51.34	222.83	331.92	50.67	36.92
2% TONC/PVA	50.95	222.64	330.09	61.89	45.56
4% TONC/PVA	52.01	219.25	326.90	25.47	19.14
6% TONC/PVA	50.20	217.60	326.07	23.92	18.35

Tg is the glass transition temperature, Tm_1 and Tm_2 is the melting temperature peaks, ΔHm is the melting enthalpy and Xc is the calculated crystallinity of the samples.

3.3. FT-IR analysis

FT-IR is an important technique that has been used in determining chemical structural changes of nanocellulose composites that occur during processing. Fig. 5a–c shows a representation of the FT-IR spectra

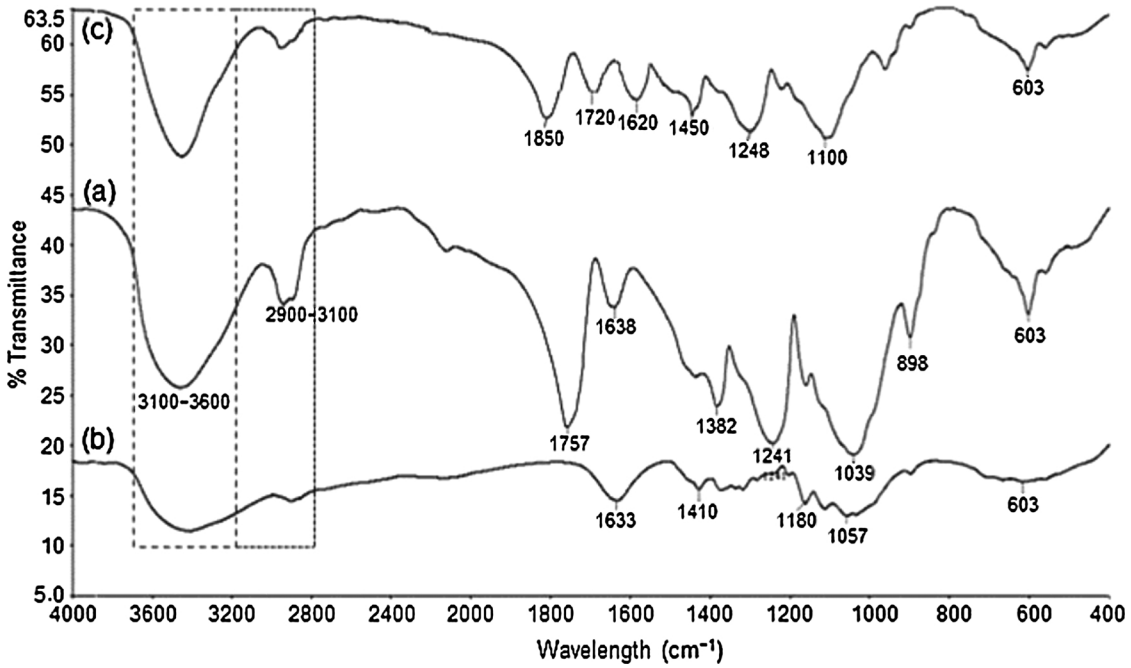

Fig. 5. FTIR spectra of (a) TONC, (b) PVA, and (c) 2% (w/w) TONC content reinforced PVA-based composite film.

of TONC, PVA TONC/PVA composite films. Abroad and wide stretching peak appearing at 3100–3600 cm^{-1} is assigned to the OH group. The additional peak at around 2900–3100 cm^{-1} assigned to overlapping symmetric and asymmetric C—H stretching vibration of the aliphatic chain in the spectrum (Han, Guenier, Salmieri, & Lacroix, 2008). In Fig. 5a, TONC exhibited a sharp asymmetric stretching peak at 1757 cm^{-1} which is designated to the hydroxyl group of OPEFB cellulose, which has been substituted by a carboxylate group (C═O) using the oxidation process. The absorption peaks at around 1100 cm^{-1} assigned to C—O stretching, 1450 and 898 cm^{-1} attributes to the H—O—H stretching vibration of absorbed water molecules and C—H stretching vibration of cellulose respectively. It is clearly revealed in the stretching vibration peaks at 1633, 1410, 1180 and 1057 cm^{-1} associated to PVA in the spectrum (Fig. 5b). The other peaks at 850 and 615 cm^{-1} assigned out of plane vibrations of O—H and C—H in PVA (Morimune, Nishino, & Goto, 2012). The slight differences can be observed after 2% (w/w) TONC addition into PVA. Indeed, the intensity and width of vibrations decreased after addition of TONC (Fig. 5c). The O—H peak slightly shifted at 3300–3550 cm^{-1} and other peaks at 1720, 1620, 1450, and 1100 cm^{-1} had their intensity decreased with TONC concentration. However, some matrix after the addition of nanocellulose content shows the intensity of appropriate peaks increased (Khan et al., 2010). The strong peak of TONC at 1720 cm^{-1} was assigned to the carboxylate group, while the C═O peak for TONC/PVA composite shifted around 1850 cm^{-1} to indicating the hydrogen bonding between C═O of TONC and OH of PVA. This indicates that the interaction between the TONC and PVA.

3.4. ^{13}C NMR analysis

Solid-state ^{13}C NMR spectra of TONC, PVA and TONC/PVA composite films are shown in Fig. 6. The six carbon peaks of TONC appeared at 103.0 (C-1), 81.3 (C-2), 72.6 (C-3), 86.7 (C-4), 63.2 (C-5) and 173.0 (C-6) ppm, while an intense peak at position C-6 due to the carboxylate group confirms the TEMPO oxidation of cellulose in Fig. 6a (Saito, Shibata, Isogai, Suguri, & Sumikawa, 2005). The carbon C-1 has a higher chemical shift as compared to C-2, C-3, C-4 and C-5 in the region 50–120 ppm. because it is extensively attached with oxygen atoms than other carbons in TONC. Fig. 6b exhibited three broad and separated carbon peaks for PVA whereas one peak appears at 43.1 ppm due to methylene carbon and other two peaks at 62.8 and 69.1 ppm assigned to carbon as attached to OH group. The TONC/PVA composite spectra assigned to the almost similar carbon peaks as TONC and PVA in Fig. 6c. While, three carbon peaks appeared in 43.0, 63.0 and 69.4 ppm attributed to PVA and other three peaks at 87.2, 102.7 and 171.8 ppm attributed to TONC carbons as C-4, C-1 and C-6 (C═O) respectively. Remaining three peaks of TONC as C-2, C-3, C-5 not appear in the spectrum (Fig. 6c) due to the splitting of the peaks or lower content of TONC used in PVA matrix for casting the composite film. The splitting of the peaks attributes to the intramolecular hydrogen bonding between OH groups (Horii, Masuda, & Kaji, 1997).

3.5. X-ray diffraction (XRD) analysis

The structure and crystallinity of TONC, PVA and TONC/PVA composite films were studied using XRD. The XRD patterns have been compared in Fig. 7a–c. It is evident that TONC peaks appeared at $2\theta = 23.2^{\circ}$ and 29.8°, which confirms the crystalline structure of TONC. However, a sharp peak around at $2\theta = 22.7^{\circ}$ is characteristic of crystalline cellulose (Zhao et al., 2013). Usually, the crystallinity of cellulose is increased after the chemical modification due to removal of hemicellulose and lignin cellulose (Cherian et al., 2008). TONC content was incorporated into PVA for producing composite films, because PVA has semi-crystallinity and cross-linkage property (Guo et al., 2010). The diffractogram of PVA film exhibited two sharp peaks at 19.5° and 29.3° in crystalline region, in which main peak at $2\theta = 19.5^{\circ}$ characterizing to PVA crystalline phase. TONC/PVA composite film exhibited a crystalline structure, whereas the peaks at $2\theta = 18.8^{\circ}$ and 21.8° assigned to cross-linking the cellulose and PVA, and a sharp peak at $2\theta = 29.0^{\circ}$ assigned to crystalline region. This indicated that 2% (w/w) TONC content had pronounced effects on cross-linking density and crystallinity of PVA. The crystallinity of TONC/PVA composite film increased than PVA film due to strongly linking between the hydroxyl groups of materials. Researchers in their work reported that when both polymer matrix and the filler phase are hydrophilic, strong molecular interactions (hydrogen bonding or van der Waals forces) found between them. As in this study PVA is a semi-crystalline polymer bearing plenty of hydroxyl groups providing inter and intra-molecular hydrogen bonding

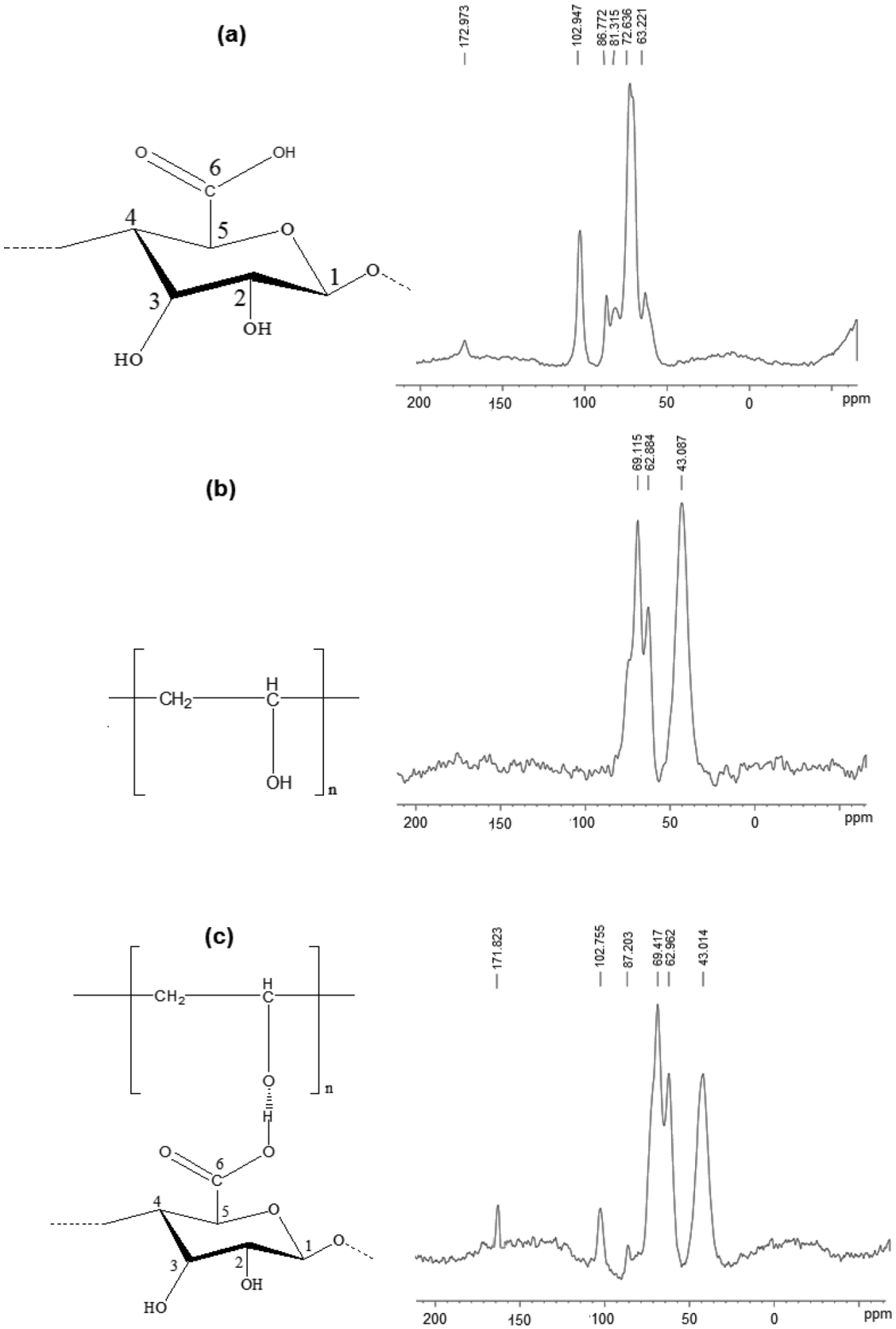

Fig. 6. ^{13}C NMR of (a) TONC, (b) PVA, and (c) 2% (w/w) TONC content reinforced PVA-based composite film.

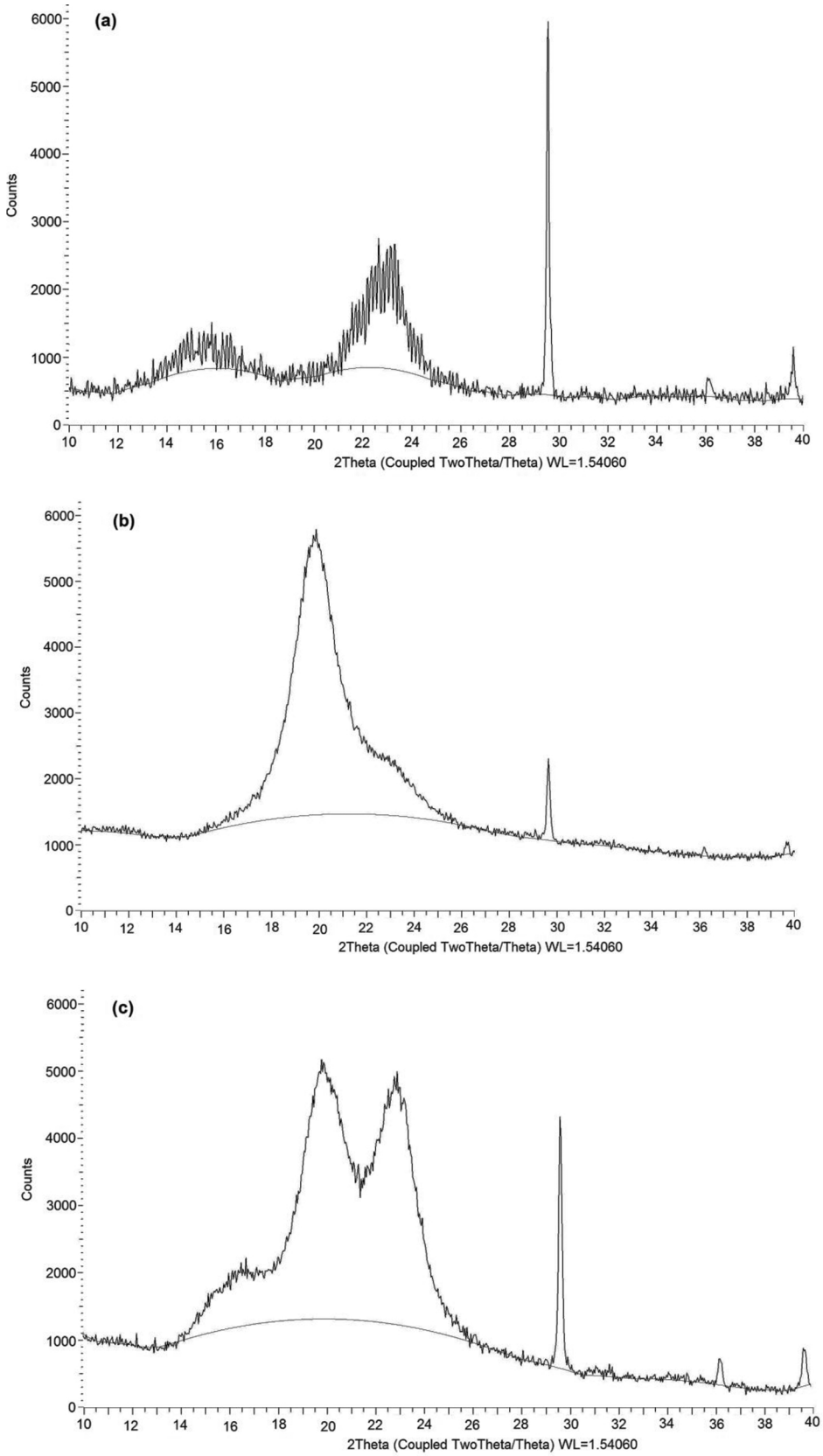

Fig. 7. XRD patterns of (a) TONC, (b) PVA, and (c) 2% (w/w) TONC content reinforced PVA-based composite film.

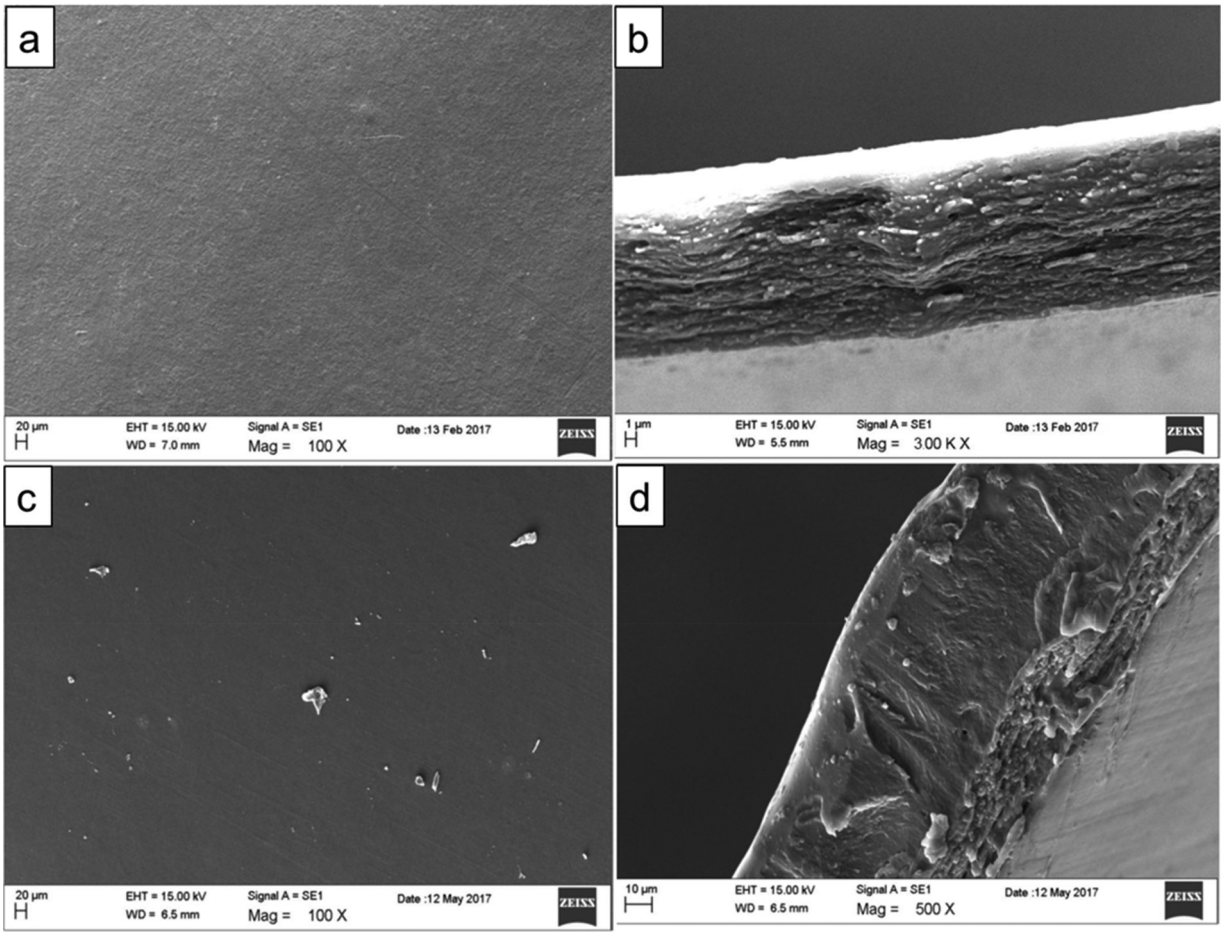

Fig. 8. SEM surface morphology of (a)TONC film, and (c) 2% (w/w) TONC content reinforced PVA-based composite film at 100× magnification, (b) Cross section of TONC film at 300×, and (d) 2% (w/w) TONC content reinforced PVA-based composite film at 500× magnification.

between TONC are expected (Voronova et al., 2015).

The crystallinity percentage of TONC, PVA, and 2%TONC/PVA composite film was calculated and observed as 81.7%, 56% and 68.4%, respectively. Relatively similar work has been reported where nanocomposite films consisting of poly (lactic acid) and NCC are being fabricated by solvent casting (Hermansson, 2012).

3.6. Morphological studies

Scanning electron microscopy (SEM) was carried out for the surface and cross section morphology investigation in TONC and TONC/PVA composite film. The surface morphology of TONC film observed as rough and slightly protruded, however cross section clearly reveals that closely packed and nano-layered phenomenon (Fig. 8a–b). PVA-based composites generally improve the properties after the addition of nanocellulose (Lee et al., 2009). It has homogenous, smooth, dense surface and other valuable structural properties. Considerable changes in morphology by the addition of TONC ascribed the intermolecular hydrogen bonding between the PVA chain and free TONC hydroxyl group. Hence, TONC/PVA composite film (Fig. 8c–d) also exhibited homogeneous, increasingly rough surface and compact structure in cross section morphology.

4. Conclusions

Nanocellulose was obtained by TEMPO oxidation of OPEFB-TCF pulp and its composite films with various concentrations were prepared by the reinforcement into a PVA matrix. FTIR and ^{13}C NMR demonstrate the structural changes and hydrogen bonding between film components. The tensile strength and Young's modulus of composite film increased considerably with increasing of TONC concentration, while the elongation at break decreased. Among the composite films, 2% (w/w) TONC film considerably enhanced the thermal stability as melting enthalpy (ΔHm = 61.89) and crystallinity (Xc = 45.56). The crystallinity percentage was also improved in XRD pattern and calculated as 81.7%, 56%, and 68.4% for TONC, PVA and 2%TONC/PVA film respectively. SEM images of TONC shows homogenous and smooth surface however reinforcement of TONC in PVA composite film shows rougher and compact structure in cross section morphology.

Acknowledgement

The financial support from Universiti Sains Malaysia through Research University Grant No. 1001/PTEKIND/**814240** is gratefully acknowledged.

References

Azizi Samir, M. A. S., Alloin, F., & Dufresne, A. (2005). Review of recent research into cellulosic whiskers, their properties and their application in nanocomposite field. *Biomacromolecules, 6*(2), 612–626. http://dx.doi.org/10.1021/bm0493685.

Brinchi, L., Cotana, F., Fortunati, E., & Kenny, J. (2013). Production of nanocrystalline-cellulose from lignocellulosic biomass: Technology and applications. *Carbohydrate Polymers, 94*(1), 154–169. http://dx.doi.org/10.1016/j.carbpol.2013.01.033.

Chang, S. H. (2014). An overview of empty fruit bunch from oil palm as feedstock for bio-oil production. *Biomass and Bioenergy, 62*, 174–181. http://dx.doi.org/10.1016/j.biombioe.2014.01.002.

Cherian, B. M., Pothan, L. A., Nguyen-Chung, T., Mennig, G., Kottaisamy, M., & Thomas, S. (2008). A novel method for the synthesis of cellulose nanofibril whiskers from banana fibers and characterization. *Journal of Agricultural and Food Chemistry, 56*(14), 5617–5627. http://dx.doi.org/10.1021/jf8003674.

Chiellini, E., Cinelli, P., Imam, S. H., & Mao, L. (2001). Composite films based on biorelated agro-industrial waste and poly(vinyl alcohol). Preparation and mechanical properties characterization. *Biomacromolecules, 2*(3), 1029–1037. http://dx.doi.org/10.1021/bm010084j.

Ferraz, N., Strømme, M., Fellström, B., Pradhan, S., Nyholm, L., & Mihranyan, A. (2012). In vitro and in vivo toxicity of rinsed and aged nanocellulose-polypyrrole composites. *Journal of Biomedical Materials Research Part A, 100A*(8), 2128–2138. http://dx.doi.org/10.1002/jbm.a.34070.

Frone, A. N., Berlioz, S., Chailan, J.-F., & Panaitescu, D. M. (2013). Morphology and thermal properties of PLA–cellulose nanofibers composites. *Carbohydrate Polymers, 91*(1), 377–384. http://dx.doi.org/10.1016/j.carbpol.2012.08.054.

Guo, Z., Zhang, D., Wei, S., Wang, Z., Karki, A. B., Li, Y., ... Ho, T. C. (2010). Effects of iron oxide nanoparticles on polyvinyl alcohol: Interfacial layer and bulk nanocomposites thin film. *Journal of Nanoparticle Research, 12*(7), 2415–2426. http://dx.doi.org/10.1007/s11051-009-9802-z.

Han, J., Guenier, A.-S., Salmieri, S., & Lacroix, M. (2008). Alginate and chitosan functionalization for micronutrient encapsulation. *Journal of Agricultural and Food Chemistry, 56*(7), 2528–2535. http://dx.doi.org/10.1021/jf703739k.

Hassan, M. L., Bras, J., Hassan, E. A., Silard, C., & Mauret, E. (2014). Enzyme-assisted isolation of microfibrillated cellulose from date palm fruit stalks. *Industrial Crops and Products, 55*, 102–108. http://dx.doi.org/10.1016/j.indcrop.2014.01.055.

Hermansson, Å. (2012). *Preparation and characterization of composite films consisting of poly (Lactic acid) and nanocrystalline cellulose. Repor No. 397*.

Horii, F., Masuda, K., & Kaji, H. (1997). CP/MAS 13C NMR spectra of frozen solutions of poly(vinyl alcohol) with different tacticities. *Macromolecules, 30*(8), 2519–2520. http://dx.doi.org/10.1021/ma961708u.

Huq, T., Salmieri, S., Khan, A., Khan, R. A., Le Tien, C., Riedl, B., ... Lacroix, M. (2012). Nanocrystalline cellulose (NCC) reinforced alginate based biodegradable nanocomposite film. *Carbohydrate Polymers, 90*(4), 1757–1763. http://dx.doi.org/10.1016/j.carbpol.2012.07.065.

Isogai, A., Saito, T., & Fukuzumi, H. (2011). TEMPO-oxidized cellulose nanofibers. *Nanoscale, 3*, 71–85.

Khan, R. A., Salmieri, S., Dussault, D., Uribe-Calderon, J., Kamal, M. R., Safrany, A., & Lacroix, M. (2010). Production and properties of nanocellulose-reinforced methylcellulose-based biodegradable films. *Journal of Agricultural and Food Chemistry, 58*(13), 7878–7885. http://dx.doi.org/10.1021/jf1006853.

Khan, A., Huq, T., Khan, R. A., Riedl, B., & Lacroix, M. (2014). Nanocellulose-based composites and bioactive agents for food packaging. *Critical Reviews in Food Science and Nutrition, 54*(2), 163–174. http://dx.doi.org/10.1080/10408398.2011.578765.

Korhonen, J. T., Kettunen, M., Ras, R. H. A., & Ikkala, O. (2011). Hydrophobic nanocellulose aerogels as floating, sustainable, reusable, and recyclable oil absorbents. *ACS Applied Materials & Interfaces, 3*(6), 1813–1816. http://dx.doi.org/10.1021/am200475b.

Lee, S.-Y., Mohan, D. J., Kang, I.-A., Doh, G.-H., Lee, S., & Han, S. O. (2009). Nanocellulose reinforced PVA composite films: Effects of acid treatment and filler loading. *Fibers and Polymers, 10*(1), 77–82. http://dx.doi.org/10.1007/s12221-009-0077-x.

Lee, K.-Y., Tammelin, T., Schulfter, K., Kiiskinen, H., Samela, J., & Bismarck, A. (2012). High performance cellulose nanocomposites: Comparing the reinforcing ability of bacterial cellulose and nanofibrillated cellulose. *ACS Applied Materials & Interfaces, 4*(8), 4078–4086. http://dx.doi.org/10.1021/am300852a.

Leh, C. P., Rosli, W. D. W., Zainuddin, Z., & Tanaka, R. (2008). Optimisation of oxygen delignification in production of totally chlorine-free cellulose pulps from oil palm empty fruit bunch fibre. *Industrial Crops and Products, 28*(3), 260–267. http://dx.doi.org/10.1016/j.indcrop.2008.02.016.

Lin, N., Bruzzese, C., & Dufresne, A. (2012). TEMPO-oxidized nanocellulose participating as crosslinking aid for alginate-based sponges. *ACS Applied Materials & Interfaces, 4*(9), 4948–4959. http://dx.doi.org/10.1021/am301325r.

Lu, J., Wang, T., & Drzal, L. T. (2008). Preparation and properties of microfibrillated cellulose polyvinyl alcohol composite materials. *Composites Part A: Applied Science and Manufacturing, 39*(5), 738–746. http://dx.doi.org/10.1016/j.compositesa.2008.02.003.

Morimune, S., Nishino, T., & Goto, T. (2012). Poly(vinyl alcohol)/graphene oxide nanocomposites prepared by a simple eco-process. *Polymer Journal, 44*(10), 1056–1063. http://dx.doi.org/10.1038/pj.2012.58.

Mulligan, C. N. (2005). Environmental applications for biosurfactants. *Environmental Pollution, 133*(2), 183–198. http://dx.doi.org/10.1016/j.envpol.2004.06.009.

Ng, H.-M., Sin, L. T., Tee, T.-T., Bee, S.-T., Hui, D., Low, C.-Y., & Rahmat, A. R. (2015). Extraction of cellulose nanocrystals from plant sources for application as reinforcing agent in polymers. *Composites Part B: Engineering, 75*, 176–200. http://dx.doi.org/10.1016/j.compositesb.2015.01.008.

Orts, W. J., Nobes, G. A. R., Glenn, G. M., Gray, G. M., Imam, S., & Chiou, B.-S. (2007). Blends of starch with ethylene vinyl alcohol copolymers: Effect of water, glycerol, and amino acids as plasticizers. *Polymers for Advanced Technologies, 18*(8), 629–635. http://dx.doi.org/10.1002/pat.869.

Park, J.-S., Park, J.-W., & Ruckenstein, E. (2001). Thermal and dynamic mechanical analysis of PVA/MC blend hydrogels. *Polymer, 42*(9), 4271–4280. http://dx.doi.org/10.1016/S0032-3861(00)00768-0.

Peppas, N. A., & Merrill, E. W. (1976). Differential scanning calorimetry of crystallized PVA hydrogels. *Journal of Applied Polymer Science, 20*(6), 1457–1465. http://dx.doi.org/10.1002/app.1976.070200604.

Rahman, M. M., Afrin, S., & Haque, P. (2014). Characterization of crystalline cellulose of jute reinforced poly (vinyl alcohol) (PVA) biocomposite film for potential biomedical applications. *Progress in Biomaterials, 3*(1), 23. http://dx.doi.org/10.1007/s40204-014-0023-x.

Rohaizu, R., & Wanrosli, W. D. (2017). Sono-assisted TEMPO oxidation of oil palm lignocellulosic biomass for isolation of nanocrystalline cellulose. *Ultrasonics Sonochemistry, 34*, 631–639. http://dx.doi.org/10.1016/j.ultsonch.2016.06.04.

Rosli, W. D. W., Leh, C. P., Zainuddin, Z., & Tanaka, R. (2003). Optimisation of soda pulping variables for preparation of dissolving pulps from oil palm fibre. *Holzforschung, 57*(1), http://dx.doi.org/10.1515/HF.2003.017.

Saito, T., Shibata, I., Isogai, A., Suguri, N., & Sumikawa, N. (2005). Distribution of carboxylate groups introduced into cotton linters by the TEMPO-mediated oxidation. *Carbohydrate Polymers, 61*(4), 414–419. http://dx.doi.org/10.1016/j.carbpol.2005.05.014.

Segal, L. C., Creely, J., Jr., Martin, A. E. J., & Conrad, C. M. (1959). An empirical method for estimating the degree of crystallinity of native cellulose using the x-ray diffractometer. *Textile Research Journal, 29*(10), 786–794. http://dx.doi.org/10.1177/004051755902901003.

Siqueira, G., Bras, J., & Dufresne, A. (2009). Cellulose whiskers versus microfibrils: Influence of the nature of the nanoparticle and its surface functionalization on the thermal and mechanical properties of nanocomposites. *Biomacromolecules, 10*(2), 425–432. http://dx.doi.org/10.1021/bm801193d.

Sorrentino, A., Gorrasi, G., & Vittoria, V. (2007). Potential perspectives of bio-nanocomposites for food packaging applications. *Trends in Food Science & Technology, 18*(2), 84–95. http://dx.doi.org/10.1016/j.tifs.2006.09.004.

Su, J.-F., Huang, Z., Yuan, X.-Y., Wang, X.-Y., & Li, M. (2010). Structure and properties of carboxymethyl cellulose/soy protein isolate blend edible films crosslinked by Maillard reactions. *Carbohydrate Polymers, 79*(1), 145–153. http://dx.doi.org/10.1016/j.carbpol.2009.07.035.

Sun, X., Lu, C., Liu, Y., Zhang, W., & Zhang, X. (2014). Melt-processed poly(vinyl alcohol) composites filled with microcrystalline cellulose from waste cotton fabrics. *Carbohydrate Polymers, 101*, 642–649. http://dx.doi.org/10.1016/j.carbpol.2013.09.088.

Tharanathan, R. (2003). Biodegradable films and composite coatings: Past, present and future. *Trends in Food Science & Technology, 14*(3), 71–78. http://dx.doi.org/10.1016/S0924-2244(02)00280-7.

Voronova, M. I., Surov, O. V., Guseinov, S. S., Barannikov, V. P., & Zakharov, A. G. (2015). Thermal stability of polyvinyl alcohol/nanocrystalline cellulose composites. *Carbohydrate Polymers, 130*, 440–447. http://dx.doi.org/10.1016/j.carbpol.2015.05.032.

Wanrosli, W. D., Zainuddin, Z., & Lee, L. K. (2004). Influence of pulping variables on the properties of Elaeis guineensis soda pulp as evaluated by response surface methodology. *Wood Science and Technology, 38*(3), 191–205. http://dx.doi.org/10.1007/s00226-004-0227-7.

Wanrosli, W. D., Rohaizu, R., & Ghazali, A. (2011). Synthesis and characterization of cellulose phosphate from oil palm empty fruit bunches microcrystalline cellulose. *Carbohydrate Polymers, 84*(1), 262–267. http://dx.doi.org/10.1016/j.carbpol.2010.11.032.

Yan, C., Wang, J., Kang, W., Cui, M., Wang, X., Foo, C. Y., ... Lee, P. S. (2014). Highly stretchable piezoresistive graphene-nanocellulose nanopaper for strain sensors. *Advanced Materials, 26*(13), 2022–2027. http://dx.doi.org/10.1002/adma.201304742.

Zhang, X., Burgar, I., Lourbakos, E., & Beh, H. (2004). The mechanical property and phase structures of wheat proteins/polyvinyl alcohol blends studied by high-resolution solid-state NMR. *Polymer, 45*(10), 3305–3312. http://dx.doi.org/10.1016/j.polymer.2004.02.044.

Zhang, W., He, X., Li, C., Zhang, X., Lu, C., Zhang, X., & Deng, Y. (2014). High performance poly (vinyl alcohol)/cellulose nanocrystals nanocomposites manufactured by injection molding. *Cellulose, 21*(1), 485–494. http://dx.doi.org/10.1007/s10570-013-0141-y.

Zhao, J., Zhang, W., Zhang, X., Zhang, X., Lu, C., & Deng, Y. (2013). Extraction of cellulose nanofibrils from dry softwood pulp using high shear homogenization. *Carbohydrate Polymers, 97*(2), 695–702. http://dx.doi.org/10.1016/j.carbpol.2013.05.050.

Zimmermann, T., Pöhler, E., & Geiger, T. (2004). Cellulose fibrils for polymer reinforcement. *Advanced Engineering Materials, 6*(9), 754–761. http://dx.doi.org/10.1002/adem.200400097.